Supplementary Materials:

Locking status and earthquake potential hazard along the middle-south Xianshuihe fault

Rumeng Guo [1,2,3], Yong Zheng [2,*], Wen Tian [1,3], Jianqiao Xu [1], Wenting Zhang [4]

[1] State Key Laboratory of Geodesy and Earth's Dynamics, Institute of Geodesy and Geophysics, Chinese Academy of Sciences, Wuhan 430077, China; guorm@asch.whigg.ac.cn

[2] State Key Laboratory of Geological Processes and Mineral Resources, Institute of Geophysics and Geomatics, China University of Geosciences, Wuhan 430074, China

[3] College of Earth Sciences, University of Chinese Academy of Sciences, Beijing 100049, China

[4] The Second Monitoring and Application Center, China Earthquake Administration, Xi'an 710054, China

***** Correspondence: **zhengyong@cug.edu.cn**

Text S1

We estimate the surface displacements caused by viscoelastic stress relaxation based on a forward modeling. Assuming that strain rate does not play a major role, we use an effective Newtonian Maxwell and/or Standard Linear Solid (SLS) rheology to represent candidate viscosity structures. The SLS body is composed by a Maxwell element in parallel with a spring, and the Maxwell body is a special case of SLS body. The shear modulus for the SLS rheology is defined by Ben-Menahem and Singh [1]:

$$\mu(iw) = \mu_2 \frac{\alpha\mu_2 + (1-\alpha)iw\eta}{\mu_2 + (1-\alpha)iw\eta} \tag{1}$$

where μ_2 represents the unrelaxed modulus, η is viscosity, and w represents frequency. The fully relaxed modulus is described as: $\frac{\mu_1\mu_2}{\mu_1 + \mu_2}$, that is $\alpha\mu_2$, where $\alpha\left(= \frac{\mu_1}{\mu_1 + \mu_2}\right)$ is a ratio between the effective and the unrelaxed shear modulus, varying between 0 and 1. Here, μ_1 represents shear modulus of the parallel spring element. When $\alpha = 0$, the rheological model reveals a Maxwell rheology, and for $0 < \alpha < 1$, it represents the SLS rheology, whereas for $\alpha = 1$, the medium is perfectly elastic (Kelvin rheology). We can estimate the time-dependent post-seismic displacements associated with viscoelastic relaxation by putting equation (1) into the Hooke's linear constitutive relation [2].

Text S2

Freed [3] proposed that faults that lie in areas of positive CFS changes are brought close to failure. Therefore, we estimate the changes of CFS caused by the co-seismic rupture and post-seismic viscoelastic stress relaxation process using PSGRN/PSCMP code [4, 5]. In this study, the changes of CFS (ΔCFS) was described in equation (1):

$$\Delta CFS = \Delta\tau_s + \mu\Delta\sigma_n \tag{2}$$

where $\Delta\tau_s$ is the change of shear stress and $\Delta\sigma_n$ is the change in normal stress. The effective friction coefficient μ is set to be 0.4 [6], which is same as Shan et al. [4]. Here, the segment between Daofu County and Kangding City were used as our receiver fault. We use the same seismic slip distribution as section 3 as our input model. In addition, we test the sensitivity of the calculations to changes in the friction coefficient and found no qualitative impact. Similar phenomena were also detected by Bedford et al. [7]. We also find that viscosities do not strongly affect the stress changes induced by post-seismic relaxation [4].

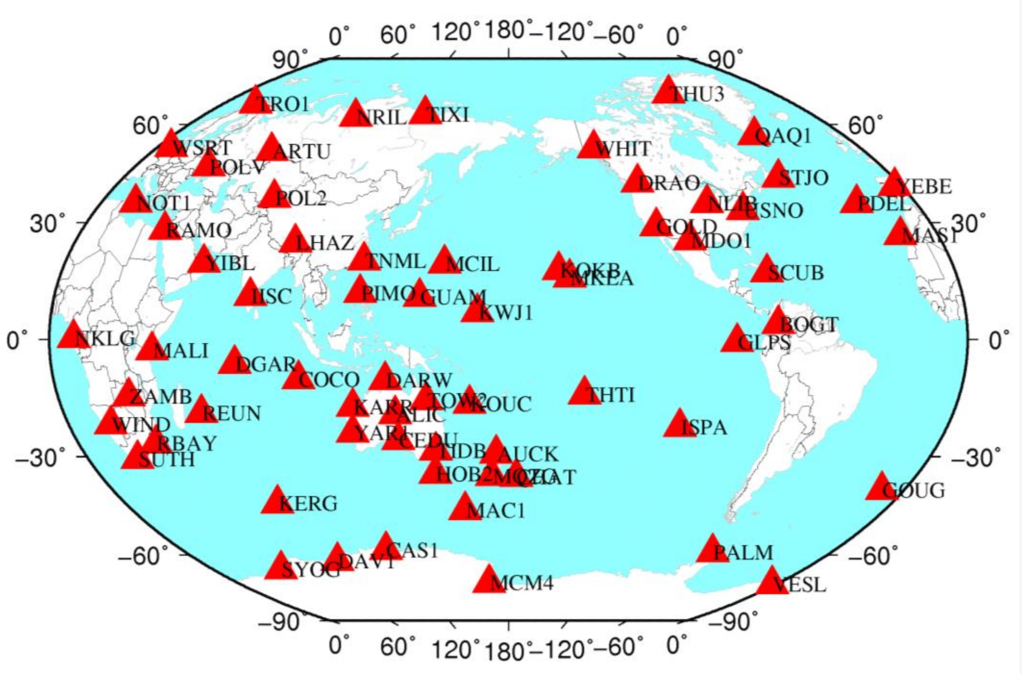

Figure S1. IGS sites for the ITRF2008 framework.

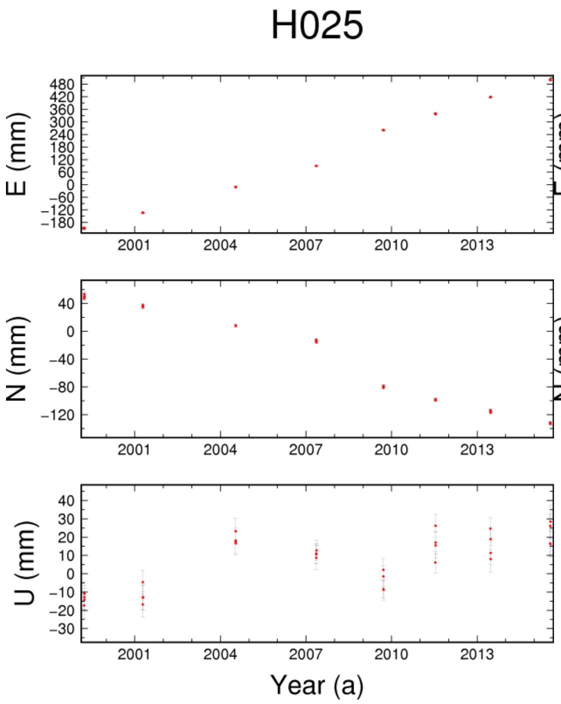
H025
E (mm)
N (mm)
U (mm)
2001
2004
2007
2010
2013
Year (a)

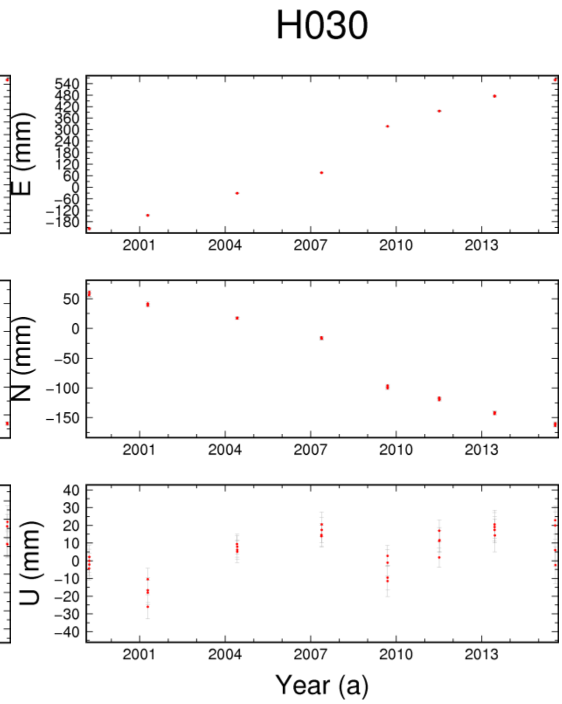
H030
E (mm)
N (mm)
U (mm)
2001
2004
2007
2010
2013
Year (a)

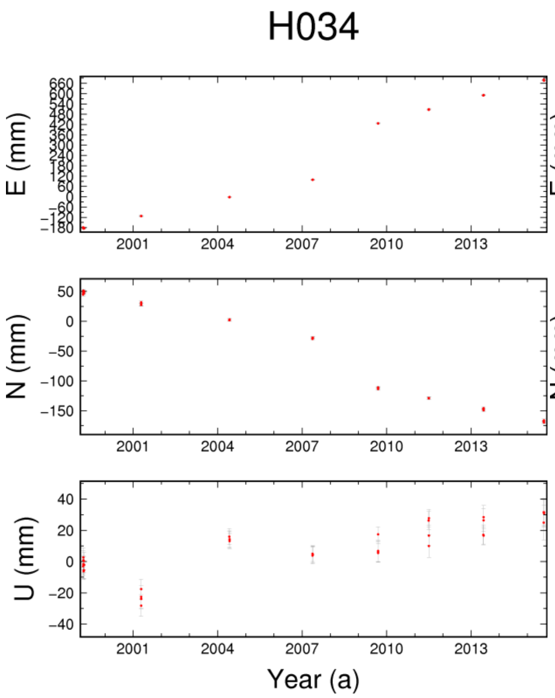
H034
E (mm)
N (mm)
U (mm)
2001
2004
2007
2010
2013
Year (a)

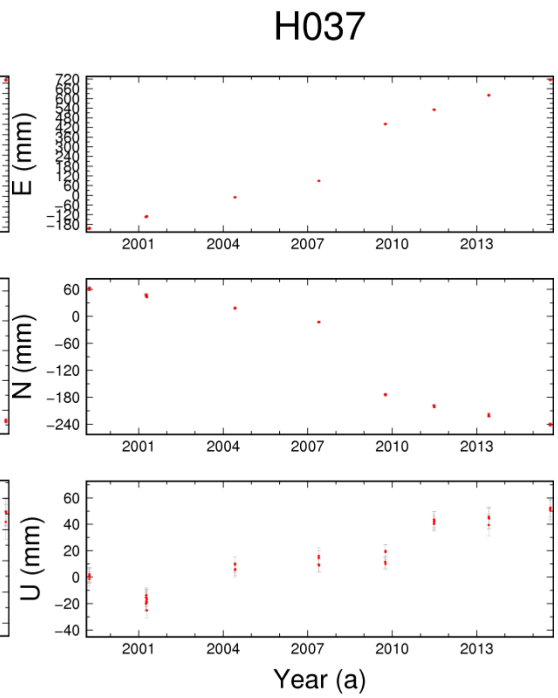
H037
E (mm)
N (mm)
U (mm)
2001
2004
2007
2010
2013
Year (a)

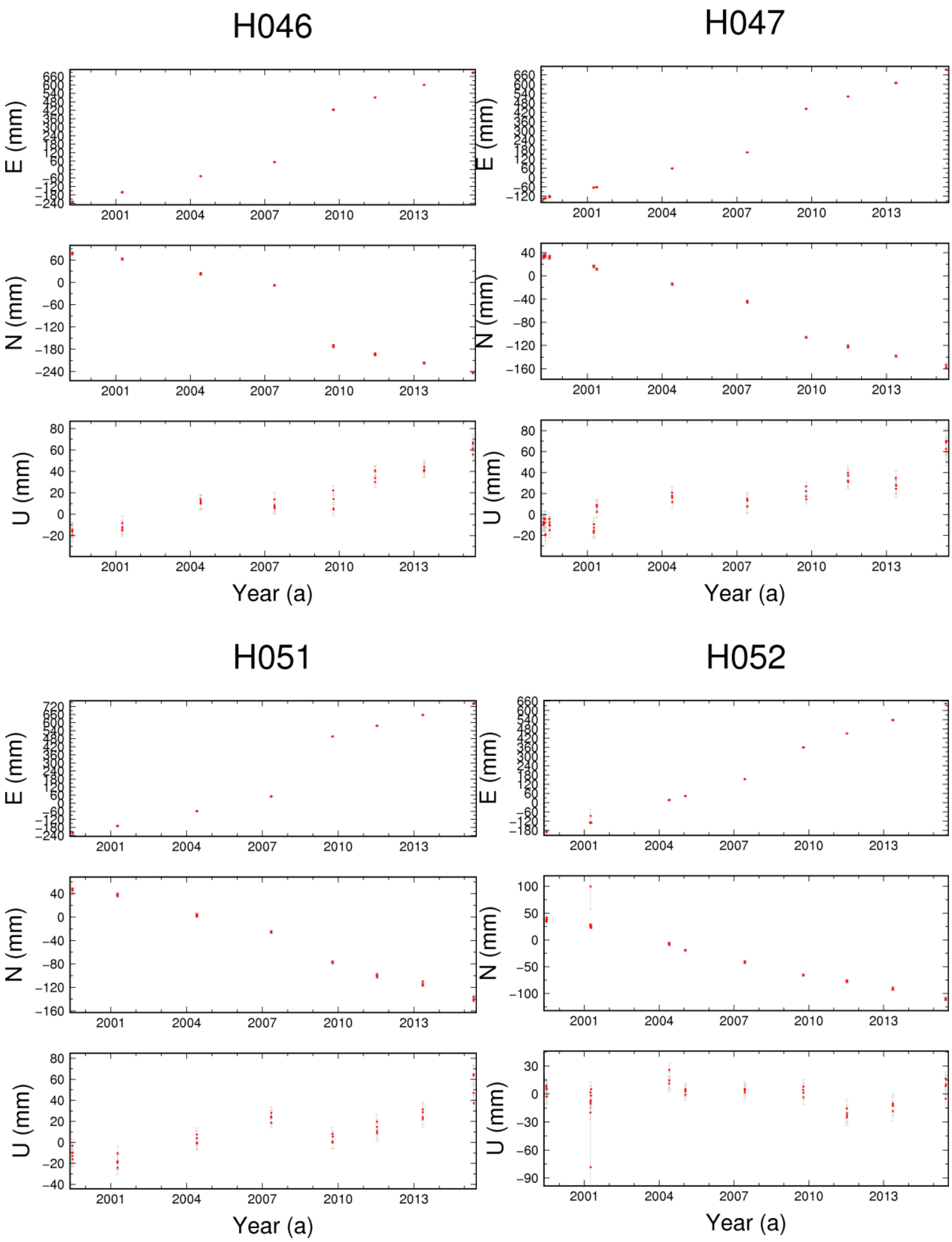
H046
H047
H051
H052
E (mm)
N (mm)
U (mm)
2001
2004
2007
2010
2013
Year (a)

H053

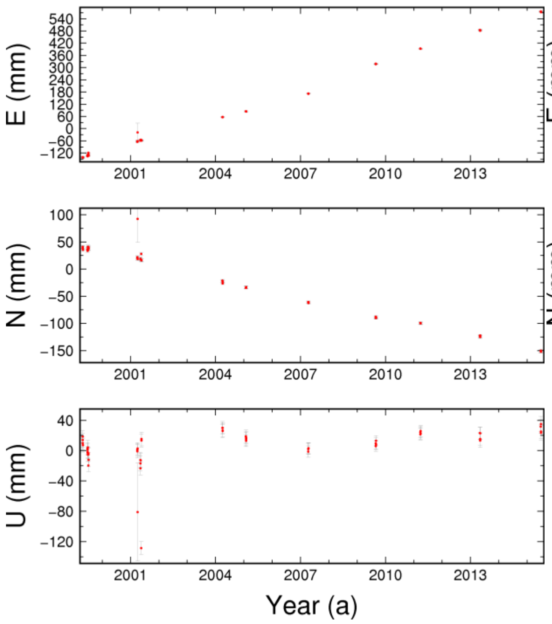

H066

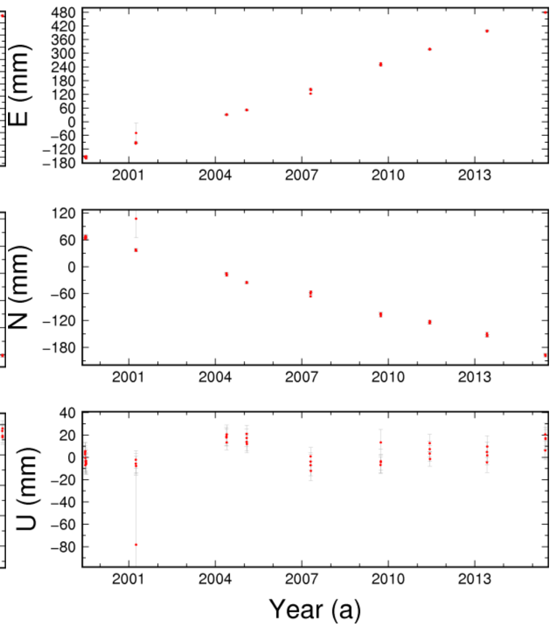

H067

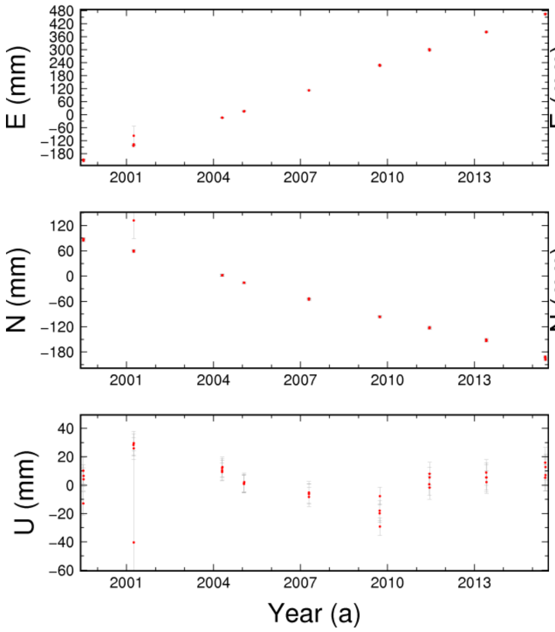

H068

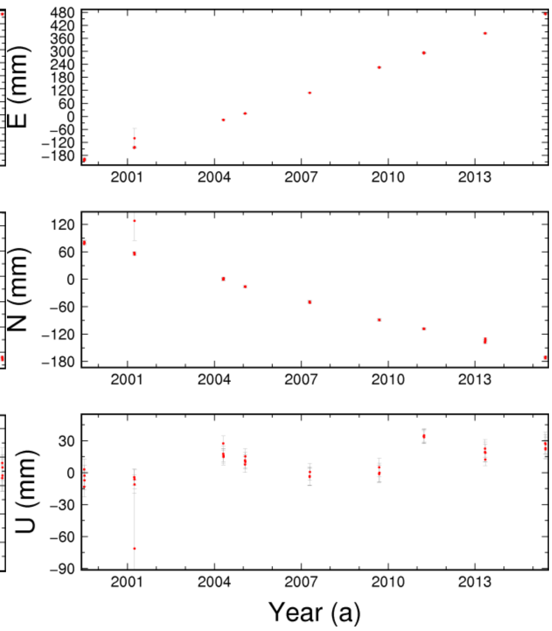

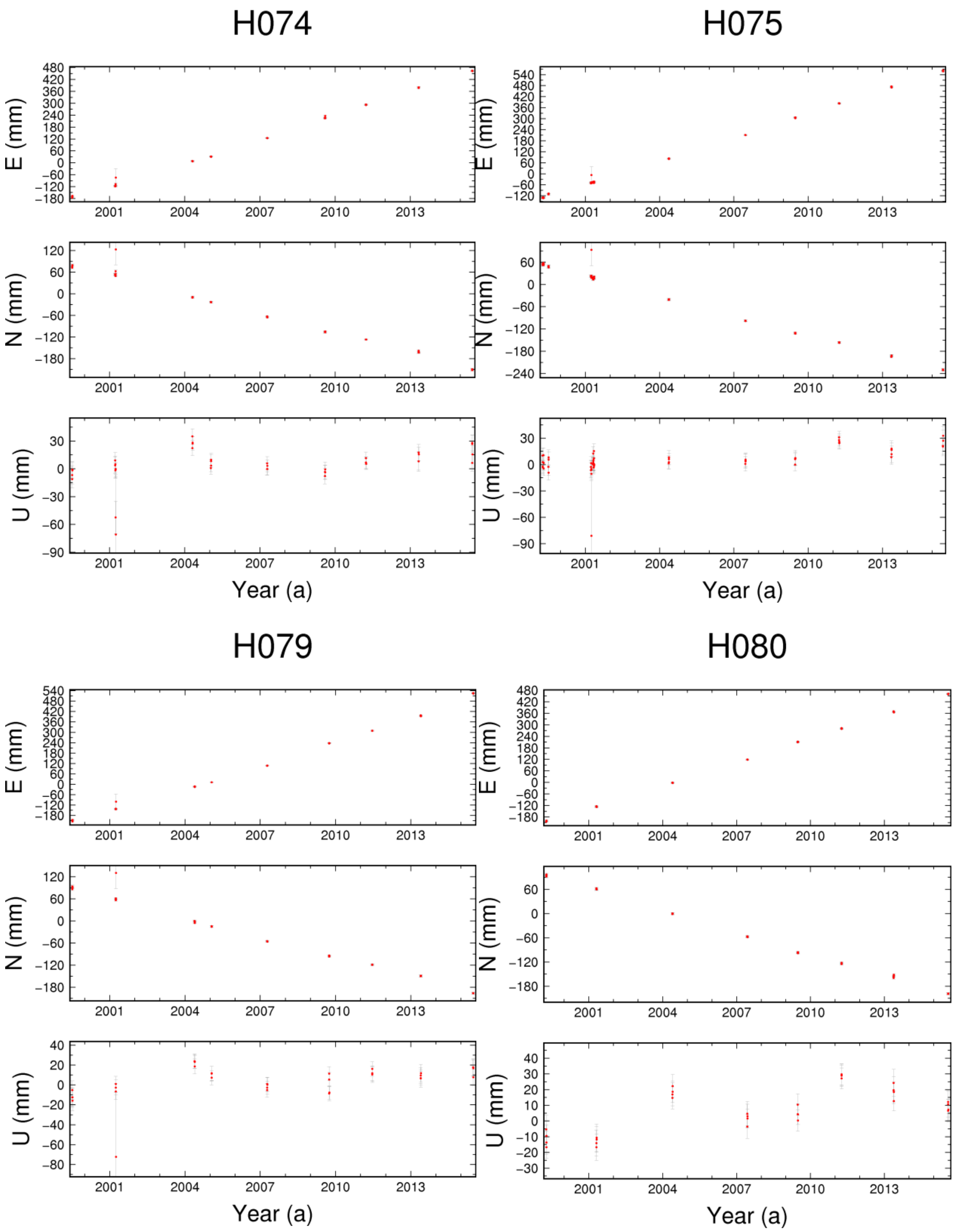
H074
H075
H079
H080
E (mm)
N (mm)
U (mm)
Year (a)

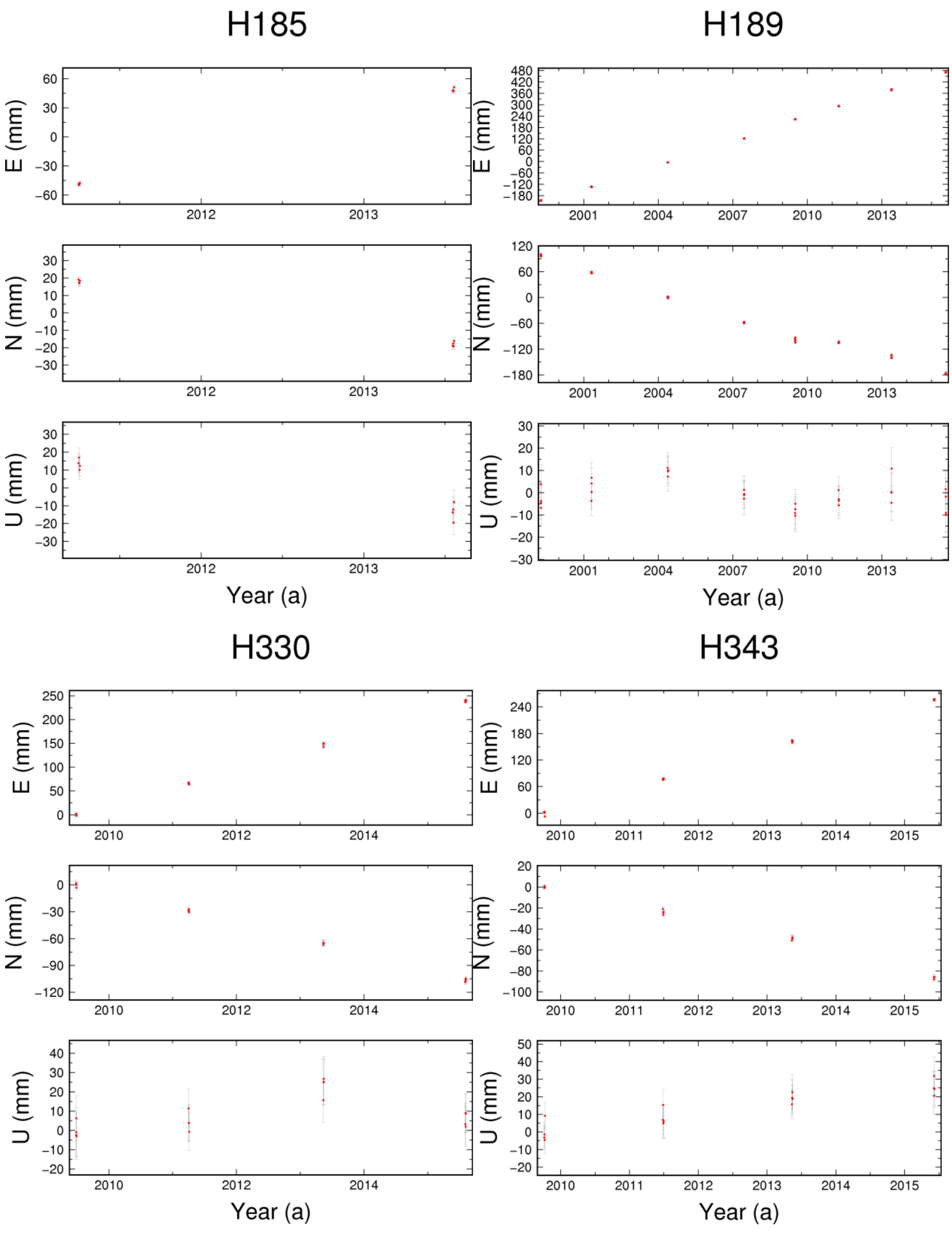

H185
H189
H330
H343
E (mm)
N (mm)
U (mm)
Year (a)

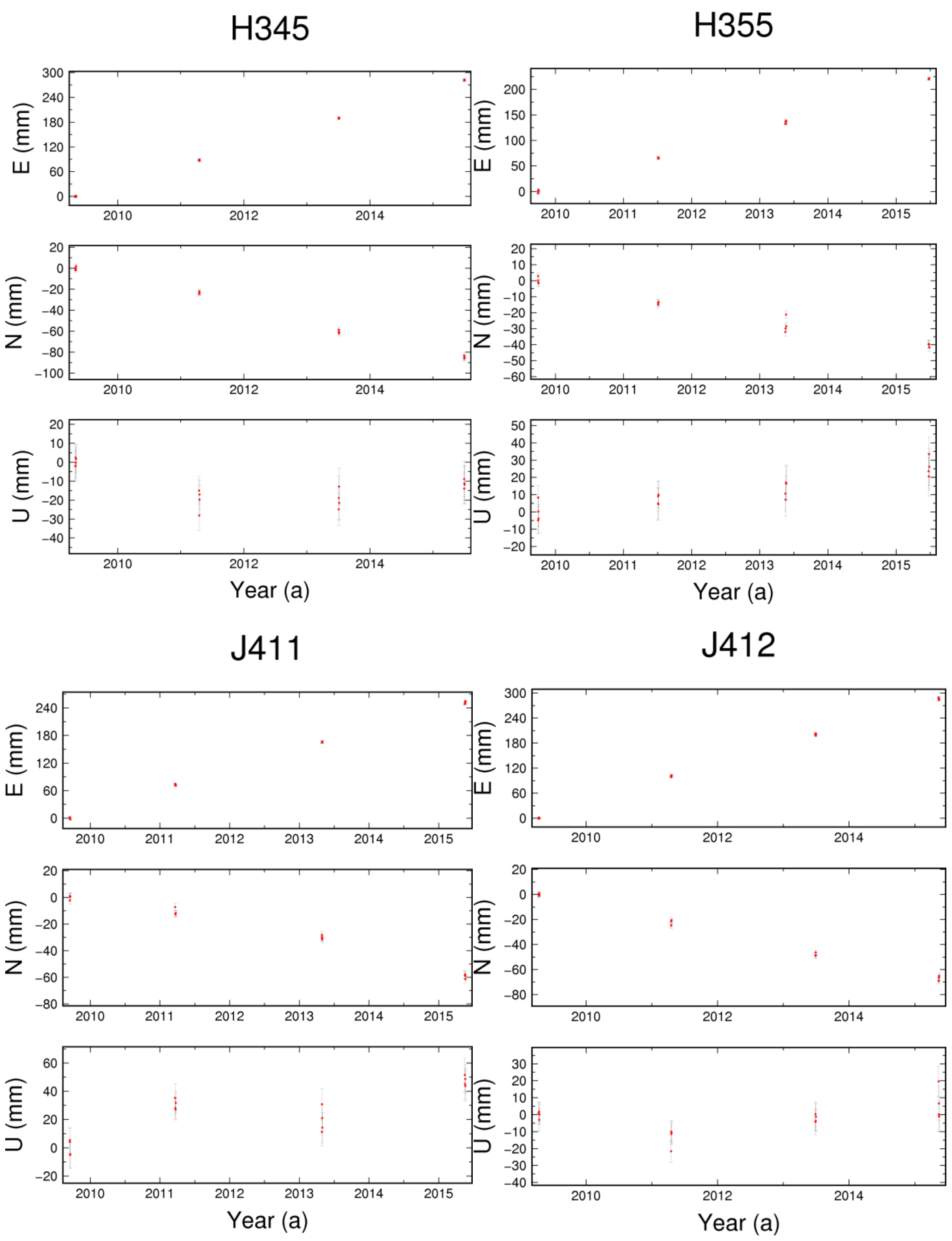
H345
H355
J411
J412
E (mm)
N (mm)
U (mm)
Year (a)

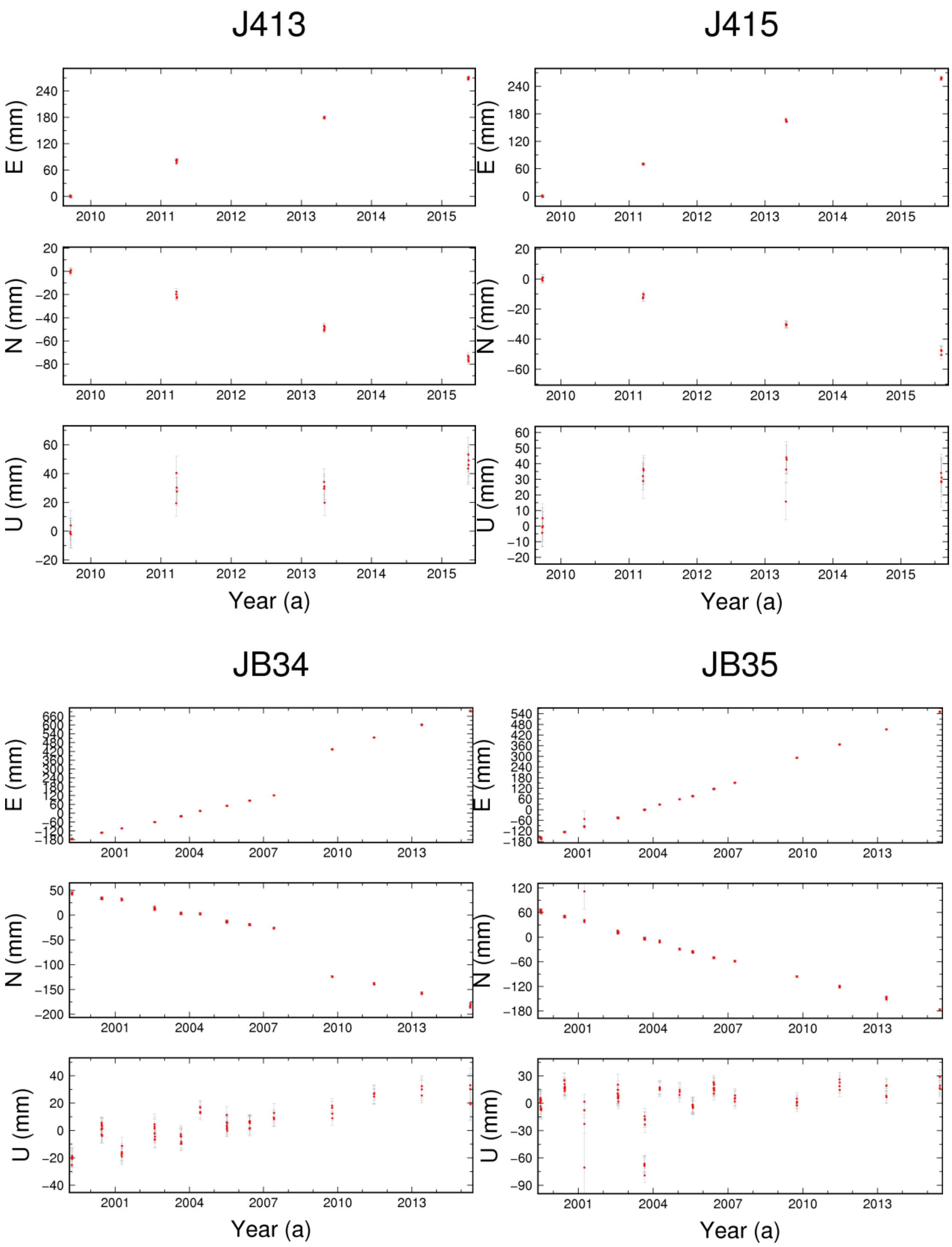

J413
J415
JB34
JB35
E (mm)
N (mm)
U (mm)
Year (a)

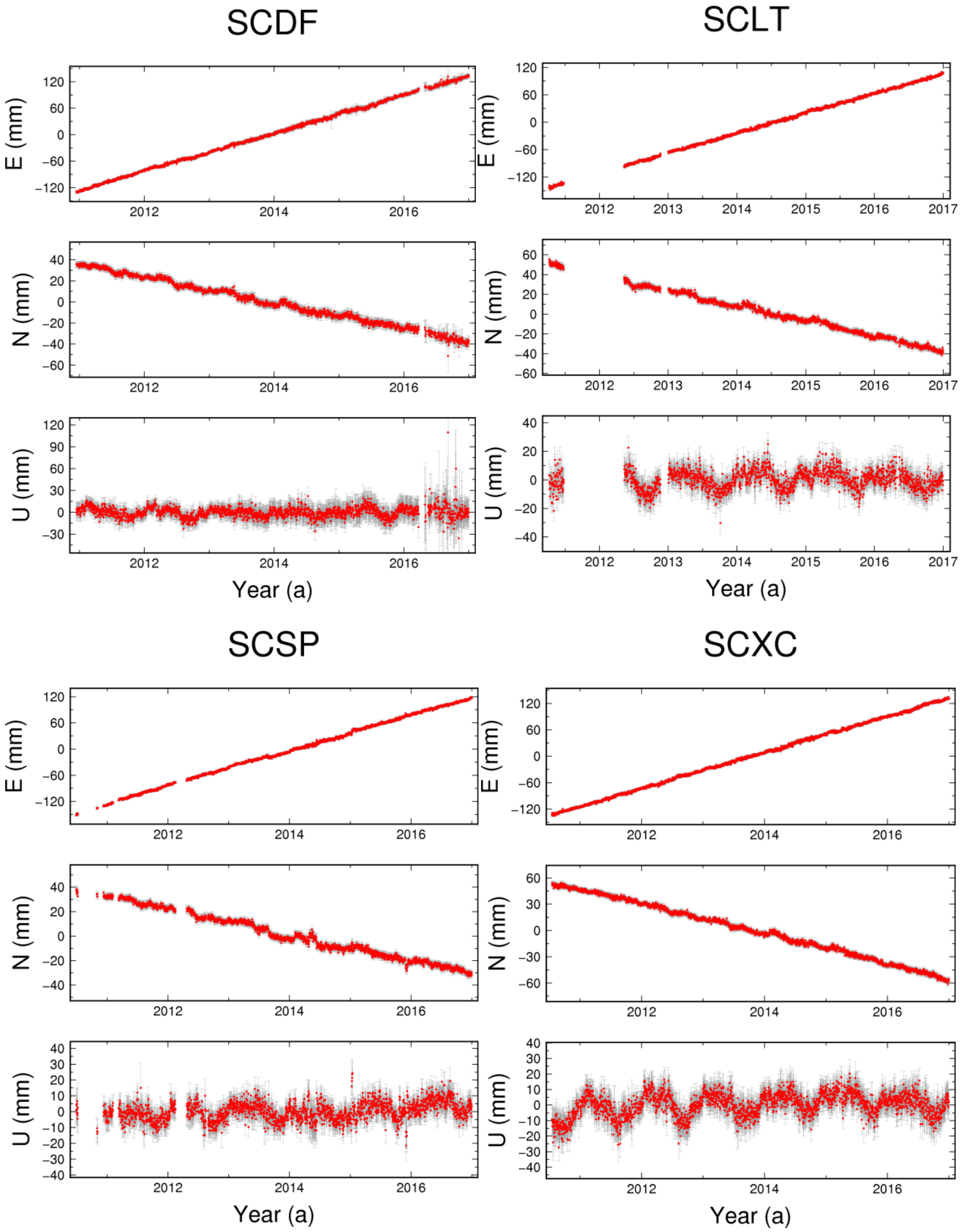

SCDF
SCLT
SCSP
SCXC
E (mm)
N (mm)
U (mm)
Year (a)
2012
2013
2014
2015
2016
2017

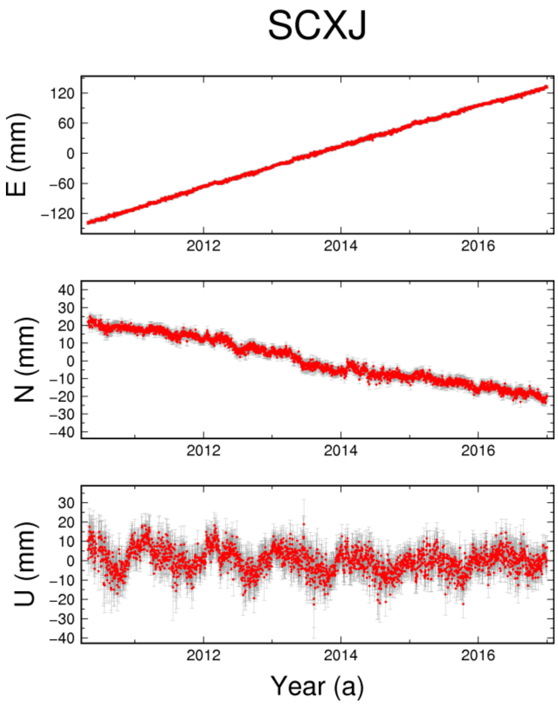

Figure S2. Displacements time series relative to ITRF2008 used in this work. The red points show the interseismic displacements with error bars of 95% confidence.

Table S1. GPS stations used in this work

Project	Time Span	Number	Surveying Mode	Station
Continuous Stations of CMONOC II	2010-2017	5	Sampling rate: 30 s	SCDF, SCLT, SCSP, SCXC, and SCXJ
Campaign-mode Stations of CMONOC I	1999-2015	19	Sampling rate:30 s, observed in 1999, 2001, 2003, 2004, 2007, 2009, 2011, 2013, and 2015, with an occupation of 3-5 days for each station	H025, H030, H034, H037, H046, H047, H051, H052, H053, H066, H067, H068, H074, H075, H079, H080, H189, JB34, and JB35
Campaign-mode Stations of CMONOC II	2009-2015	9	Sampling rate: 30 s, observed in 2009, 2011, 2013, and 2015, with an occupation of 3-5 days for each	H185, H330, H343, H345, H355, J411, J412, J413, and J415

			station	

Table S2. GPS velocities used in this work (mm/a)

Num.	Sta.	Long.	Lat.	Ve		σ_n	Vn		σ_e
				ITRF2008	Eurasia Fixed Reference Frame		ITRF2008	Eurasia Fixed Reference Frame	
1	H025	103.43458	32.93072	36.6	8.313	0.2	-8.0	-2.049	0.1
2	H030	103.61268	32.59076	37.8	9.515	0.7	-9.7	-3.705	0.3
3	H034	103.73196	32.36148	36.8	8.517	1.3	-9.4	-3.376	0.1
4	H037	103.16571	32.07503	39.7	11.380	1.8	-9.9	-4.015	0.5
5	H046	102.67030	31.85038	34.2	5.849	0.2	-10.4	-4.638	0.4
6	H047	102.09559	31.46642	37.7	9.314	0.7	-9.5	-3.881	0.1
7	H051	102.77452	30.99181	37.6	9.245	1.5	-9.9	-4.112	0.4
8	H052	101.86601	30.94935	45.5	16.998	0.8	-10.1	-4.539	0.2
9	H053	101.16291	30.95540	40.2	11.764	0.6	-12.6	-7.215	0.3
10	H066	101.78834	30.07411	38.8	10.393	0.3	-17.0	-11.458	0.5
11	H067	101.48570	30.07506	41.7	13.278	0.1	-18.8	-13.334	0.3
12	H068	101.02303	30.10621	41.3	12.856	0.5	-16.5	-11.150	0.5
13	H074	101.55841	29.84641	39.3	10.882	0.3	-18.9	-13.415	0.3
14	H075	100.39007	29.69548	41.3	12.829	0.2	-18.5	-13.309	0.1
15	H079	101.52424	30.32563	44.6	16.180	1.8	-18.2	-12.724	0.5
16	H080	100.12082	29.17543	39.8	11.322	0.3	-17.5	-12.337	0.6
17	H185	100.27791	29.99308	42.2	13.722	0.7	-15.6	-10.437	0.6
18	H189	99.74483	29.00026	40.9	12.408	0.3	-16.8	-11.772	1.3
19	H330	100.34251	28.55900	38.7	10.240	0.3	-17.2	-12.021	0.2

20	H343	101.06536	30.57220	45.4	16.958	0.7	-16.7	-11.339	0.2
21	H345	101.40432	30.61207	45.4	16.974	0.3	-12.5	-7.054	0.3
22	H355	101.75441	30.62142	39.2	10.791	0.4	-6.5	-0.966	0.5
23	J411	102.14146	31.94150	43.5	15.123	0.3	-11.1	-5.470	0.4
24	J412	102.50200	31.35251	47.0	18.634	0.5	-11.1	-5.380	0.2
25	J413	102.83289	31.63766	45.8	17.455	0.4	-13.2	-7.398	0.3
26	J415	103.67602	31.97694	42.8	14.506	0.6	-7.5	-1.489	0.4
27	JB34	102.30608	31.70572	36.8	8.428	0.3	-8.9	-3.229	0.2
28	JB35	101.49658	30.49475	40.9	12.478	0.5	-16.1	-10.631	0.3
29	SCDF	101.12271	30.97789	43.1	14.662	0.2	-12.1	-6.725	0.1
30	SCLT	100.21810	29.99165	43.5	15.020	0.1	-15.2	-10.052	0.1
31	SCSP	103.58241	32.64843	40.4	12.114	0.3	-10.6	-4.612	0.2
32	SCXC	99.80324	28.93738	41.0	12.511	0.1	-17.0	-11.957	0.1
33	SCXJ	102.37213	31.00038	40.6	12.224	0.3	-6.6	-0.912	0.3

Table S3. The geological and geodetic slip rate of the SDK (mm/a)

Number	**Data Source**		**Slip Rate**
1	Geological Investigation	Allen et al. [21]	10±5
2		Chen et al. [30]	6.7~17
3		Zhang [16]	8.0~11.0
4	Geodetic Measurements	Shen et al [5] (1998-2004)	10±2
5		Zhang [32] (1998-2004)	10±1.5
6		Jiang et al. [1] (1999-2013, 19)	7.0~7.6

7		This study (1999-2017, 33)	7.8±0.4

1. Ari, B.-M.; Singh, S.J. Seismic waves and sources; Springer-Verlag New York Inc., **1981**;
2. Wang, L.; Wang, R.; Roth, F.; Enescu, B.; Hainzl, S.; Ergintav, S. Afterslip and viscoelastic relaxation following the 1999 M 7.4 Izmit earthquake from GPS measurements. *Geophysical Journal International* **2009**, 178, 1220–1237.
3. Freed, A. M. Earthquake triggering by static, dynamic, and postseismic stress transfer, *Annual Review of Earth and Planetary Sciences* **2005**, 33, 335–367.
4. Shan, B.; Xiong, X.; Wang, R.; Zheng, Y.; Yang, S. Coulomb stress evolution along Xianshuihe–Xiaojiang Fault System since 1713 and its interaction with Wenchuan earthquake, May 12, 2008. *Earth Planet Sci Lett* **2013**, *377*, 199–210.
5. Wang, R.; Lorenzo-Martín, F.; Roth, F. PSGRN/PSCMP—a new code for calculating co-and post-seismic deformation, geoid and gravity changes based on the viscoelastic-gravitational dislocation theory. *Computers & Geosciences* **2006**, 32, 527–541.
6. Parsons, T.; Stein, R.S.; Simpson, R.W.; Reasenberg, P.A. Stress sensitivity of fault seismicity: A comparison between limited-offset oblique and major strike-slip faults. *Journal of Geophysical Research: Solid Earth* **1999**, 104, 20183–20202.
7. Bedford, J.; Moreno, M.; Baez, J.C.; Lange, D.; Tilmann, F.; Rosenau, M.; Heidbach, O.; Oncken, O.; Bartsch, M.; Rietbrock, A. A high-resolution, time-variable afterslip model for the 2010 Maule Mw= 8.8, Chile megathrust earthquake. *Earth and Planetary Science Letters* **2013**, 383, 26–36.